

# Dust-driven winds and mass loss of C-rich AGB stars with subsolar metallicities

A. Wachter<sup>1,2</sup>, J. M. Winters<sup>3</sup>, K.-P. Schröder<sup>4</sup>, and E. Sedlmayr<sup>1</sup>

<sup>1</sup> Zentrum für Astronomie und Astrophysik (ZAA), Technische Universität Berlin, Hardenbergstr. 36, 10623 Berlin, Germany  
e-mail: awachter@physik.tu-berlin.de

<sup>2</sup> Department of Physics and Astronomy, Division of Astronomy and Space Physics, Uppsala University, Box 515, 75120 Uppsala, Sweden

<sup>3</sup> Institut de RadioAstronomie Millimétrique (IRAM), 300 rue de la Piscine, Domaine Universitaire, 38406 Saint Martin d'Hères, France

<sup>4</sup> Departamento de Astronomia de la Universidad de Guanajuato, Apartado Postal 144, C.P. 36000, Guanajuato, GTO, Mexico

Received 02 April 2008 / Accepted 21 May 2008

## ABSTRACT

*Aims.* We investigate the mass loss of highly evolved, low- and intermediate mass stars and stellar samples with subsolar metallicity. We give a qualitative as well as quantitative description which can be applied to LMC/SMC-type stellar populations.

*Methods.* For that purpose we apply the same approach as we did for solar metallicity stars and calculate hydrodynamical wind models including dust formation with LMC and SMC abundances under consideration of an adapted model assumption. In particular, we improved the treatment of the radiative transfer problem in order to accommodate larger non-local contributions occurring with smaller opacities. For each wind model we determine an averaged mass-loss rate. The resulting, approximate mass-loss formulae are then applied to well-tested and calibrated stellar evolution calculations in order to quantify the stellar mass loss.

*Results.* The dynamical models for LMC and SMC metallicity result in mass-loss rates of the same order of magnitude as the solar metallicity models which is in this basic approach in agreement with observations. The hydrodynamical properties like e.g. the outflow velocity differ (for fixed C/O abundance ratio) noticeably, though. While critical luminosities of LMC and solar metallicity models fairly coincide, the SMC models need higher luminosities to develop dust-driven winds.

**Key words.** Hydrodynamics – Stars: AGB and post-AGB – Stars: carbon – Stars: evolution – Stars: late-type – Stars: mass-loss

## 1. Introduction

On the asymptotic giant branch (AGB) stars with low- and intermediate main sequence mass ( $\sim 1 \dots 8 M_{\odot}$ , precise values depend on the initial element abundances / metallicity and are as well model dependent) are in their late stage of evolution. This phase is characterised by instabilities leading to stellar pulsations as observed in long-period variables (LPVs) or Mira stars. Cioni et al. (2001), for instance, found that 65% of the stars in the considered sample of giants in the Large Magellanic Cloud (LMC) are LPVs. Furthermore, this phase is connected to strong mass-loss of more than a few  $10^{-5} M_{\odot} \text{ yr}^{-1}$ . By means of their mass loss, these stars contribute significantly to the enrichment of the interstellar matter with material processed through nuclear burning reactions in the form of molecules and dust, and are therefore not only interesting as objects of stellar evolution but also in terms of galactic chemical evolution. In this paper we extend our set of models with solar element composition (apart from the C/O ratio) to subsolar metallicities. We are using abundances as observed in the Magellanic Clouds (see table A.1 in Helling et al., 2000). The metallicity of the Large Magellanic Cloud (LMC) is  $Z = 0.008$ , i.e. roughly a good third of the solar value, while the Small Magellanic Cloud (SMC) has on average an even lower metallicity of  $Z = 0.004$ .

## 2. Dust-driven Wind Models

We base our description of the mass loss of late AGB stars with less than solar metallicities on time dependent hydrodynamical wind models that include the formation of dust grains which, by radiation pressure, drive the massive outflows. These models have been developed in the last decade by Gauger et al. (1990), Fleischer et al. (1992), Winters et al. (1994, 2000), Jeong et al. (2003).

For (apart from the C/O abundance ratio) solar abundances, these models yield time averaged mass loss rates of up to a few  $10^{-5} M_{\odot} \text{ yr}^{-1}$ , both for oxygen-rich and carbon-rich mixtures. This is consistent with rates inferred from, e.g. CO rotational line observations of AGB stars in the solar neighbourhood.

The models are obtained from the solution of the non-linearly coupled system of equations describing the hydrodynamical and thermodynamical structure of a spherically symmetric, pulsating circumstellar shell, its chemical composition, and the nucleation, growth, and evaporation of dust grains. The hydrodynamical structure (mass density  $\rho$  and outflow velocity  $v$ ) follows from the equation of continuity and the equation of motion which includes radiation pressure on dust grains. The law of energy conservation and radiative transfer determine the temperature structure. In this work we consider models with carbon-rich composition assuming that oxygen is locked in the CO molecule and assuming chemical equilibrium. The formation, growth, and evaporation of carbon grains is calculated ac-

**Table 1.** Essential input parameter ranges covered by our collection of subsolar metallicity models.

type	LMC	SMC
$L_\star [L_\odot]$	5000 ... 15000	7000 ... 12000
$T_\star [K]$	2200 ... 3200	2400 ... 3000
$M_\star [M_\odot]$	0.7 ... 1.0	0.6 ... 1.1
$\epsilon_C/\epsilon_O$	1.3/1.8	1.8
$P [d]$	325 ... 650	450 ... 650
$\Delta v [km/s]$	2/5	5

cording to the moment method developed by Gail & Sedlmayr (1988) and Gauger et al. (1990).

The equations are discretised in Lagrangian coordinates, i.e. in a co-moving coordinate system. A detailed description of the transformation and discretisation is given in Fleischer et al. (1992) and Fleischer (1994). Furthermore, a summary of the latest physical assumptions can be found in Schirmacher et al. (2003).

When applied to winds with subsolar metallicities these models show a rather quasi-static nature (Helling et al., 2002). As already pointed out by these authors, this is not consistent with observations of AGB stars, e.g. in the Magellanic Clouds which indicate mass-loss rates of the same order of magnitude as they are observed from stars with solar element abundances. Therefore, we reconsidered the model assumptions. In particular, we improved the treatment of the radiative transfer as follows:

In the solar metallicity case the shell has been considered to be optically thick so that the flux-averaged dust extinction is determined by the Planck-mean absorption coefficient at the local equilibrium temperature. However, if the atmosphere is considered to be partly transparent, the dust grains are to some extent exposed to the direct radiation from the stellar photosphere. Therefore, the flux-mean dust opacity for lower metallicity is represented by assuming a *non*-local radiation field, which is characterised by a temperature  $T$  determined according to  $T^4 = T_\star^4 e^{-\tau} + T_{\text{eq}}^4 (1 - e^{-\tau})$ , i.e. the radiation field is interpolated in optical depth  $\tau$  between the local equilibrium radiation and the stellar (black-body) radiation field (represented by  $T_{\text{eq}}$  and  $T_\star$ , respectively).

The gas opacity  $\kappa_g/\rho$  is set to a constant value of  $2 \times 10^{-4} \text{ cm}^2 \text{ g}^{-1}$  in the solar models. From figure 2 of Helling et al. (2000) it is clear that the mean gas opacity drops with lower metallicity. Therefore, we reduced the value of the gas opacity in the LMC and SMC models to  $1 \times 10^{-4}$ , and  $0.5 \times 10^{-4} \text{ cm}^2 \text{ g}^{-1}$ , respectively.

### 3. Results

Since the main purpose of this work is to derive mass-loss rates for subsolar metallicities, the focus when choosing the model parameters was primarily on covering the range of stellar parameters  $M$ ,  $L$ , and  $T$  provided by the stellar evolution code for each fixed element composition (LMC/SMC) than on performing a detailed parameter study. Nevertheless, the dependence on the carbon overabundance is shortly discussed in the following. Table 1 summarises the parameter ranges of our subsolar metallicity model sets.

Concerning the radial structure of our wind models there basically exist two different types of models:

A) models where effective dust formation and growth takes place. In this class of models the radiative acceleration on dust

exceeds the local gravitation in the region close to the stellar photosphere (typically inside of  $\approx 5R_\star$ ). In this case, the matter is lifted out of the stars' gravitational field by radiation pressure on dust, and a layered structure of the hydrodynamical and the dust quantities results in the inner part of the circumstellar shell (see, e.g., figure 1). Generally this type of models shows high mass-loss rates ( $> \text{a few } 10^{-7} M_\odot \text{ yr}^{-1}$ ) and outflow velocities in excess of  $\approx 5 \text{ km s}^{-1}$ .

B) models showing a smooth, quasi-stationary wind structure. In these model, radiation pressure on dust is not sufficient to lift the matter out of the stars' gravitational field, the resulting mass loss rates (and outflow velocities) are significantly smaller than in the type A models.

This separation has been discussed in detail in Winters et al. (2000) for the case of solar element abundances.

As the distinction between A-type and B-type models is due to the ratio of radiative to gravitational acceleration (larger or smaller than unity) in the inner shell region, the same type of separation is found for sub-solar metallicities. For the SMC and LMC models, this separation is later on considered in terms of a "critical luminosity".

In order to characterise the outflow of each time dependent wind model time-averages of several quantities are calculated. The most obvious quantities for this purpose are the mass-loss rate  $\langle \dot{M} \rangle$  and the final outflow velocity  $\langle v_\infty \rangle$ . Furthermore we consider the dust-to-gas ratio  $\langle \rho_d/\rho_g \rangle$  and the ratio of radiative to gravitational acceleration  $\langle \alpha \rangle$ , since these are expected to be significant for the general behaviour of the wind.

To calculate the averages the same procedure as used in the solar metallicity models is followed, i.e. we first average  $\dot{M}$ ,  $v$ , and  $\rho_d/\rho_g$  in the radial coordinate between 40 and 60  $R_\star$  and then over time, typically 20 periods for LMC and 80 periods for SMC models. For  $\langle \alpha \rangle$  a different procedure is followed, though. It is a time-average only, namely the average of the ratio of radiative to gravitational acceleration at the radius of the first maximum of the condensation degree, i.e. in the innermost dust layer (see, e.g., the innermost peak of  $\alpha$  in the second panel of figure 1).

#### 3.1. Influence of the C/O ratio

The C/O abundance ratio determines how much carbon is available for dust formation, since we consider carbon rich chemistry and total CO-blocking. As far as the derivation of a mass loss formula applicable for stellar evolution is concerned, the solar metallicity models already demonstrated that the mass loss rate does not depend heavily on this model parameter (see Arndt et al., 1997; Wachter et al., 2002). Instead it can be seen as a critical parameter in the sense that the mass loss rate remains the same order of magnitude once the C/O ratio is above a certain threshold.

The results of a set of calculations for LMC and SMC abundances with varying C/O ratio are summarised in table 2. In the LMC models with  $\epsilon_C/\epsilon_O = 1.3$  and 1.5 the material expands so slowly that after 110 and 90 periods the outermost grid point has just reached 10 and 25 stellar radii, respectively. This is well below the region of 40 to 60 stellar radii where we generally take the averages. The calculations have not been followed any further since the models up to that instant show a virtually stationary radial structure.

**Table 2.** Variation of the carbon overabundance  $\epsilon_{C/O}$  for otherwise fixed parameters.

$\epsilon_{C/O}$	periods	$ \dot{M} $	$\langle\alpha\rangle$	$v_\infty$	$\rho_{d/g}$	
type: LMC	$M = 0.8 M_\odot, T = 2800 \text{ K}, L = 15000 L_\odot,$ $P = 400 \text{ d}, \Delta v = 5 \text{ km s}^{-1}$					
1.30	Expansion after 110 $P: < 10 R_\star$					
1.50	Expansion after 90 $P: < 25 R_\star$					
1.70	70–90	3.51e-05	6.10	18.83	2.01e-3	
1.80	70–90	3.30e-05	3.92	21.04	2.68e-3	
2.50	70–90	4.58e-05	6.03	30.16	7.13e-3	
type: SMC	$M = 1.0 M_\odot, T = 2600 \text{ K}, L = 11000 L_\odot,$ $P = 650 \text{ d}, \Delta v = 5 \text{ km s}^{-1}$					
1.30	Expansion after 150 $P: < 35 R_\star$					
$\alpha < 1$	1.50	70–150	7.17e-07	0.06	3.23	1.69e-4
	1.70	70–150	4.74e-06	0.11	4.95	1.17e-3
$\alpha > 1$	1.80	70–150	3.69e-05	1.26	8.56	1.82e-3
	2.00	70–150	4.55e-05	2.19	10.61	2.75e-3
type: SMC	$M = 0.8 M_\odot, T = 2800 \text{ K}, L = 10000 L_\odot,$ $P = 600 \text{ d}, \Delta v = 5 \text{ km s}^{-1}$					
$\alpha < 1$	1.30	130–150	1.24e-07	0.27	1.91	1.93e-9
	1.50	70–150	8.90e-07	0.21	3.75	4.74e-4
	1.70	70–150	1.72e-05	1.02	8.31	1.27e-3
$\alpha > 1$	1.80	70–150	2.88e-05	2.04	10.57	1.75e-3
	2.00	70–150	3.76e-05	3.11	12.10	2.89e-3

**Table 3.** Mass-loss rates of SMC, LMC, and solar wind models with identical input parameters;  $\epsilon_{C/O} = 1.8, \Delta v = 5 \text{ km s}^{-1}, P = 500 \text{ d}$  at  $8000 L_\odot, 600 \text{ d}$  at  $10000 L_\odot,$  and  $700 \text{ d}$  at  $12000 L_\odot.$  Mass loss averages are over time interval 70–150 periods, or (1) 70–90, (2) 70–210.

$M$ [ $M_\odot$ ]	$T_\star$ [K]	$L_\star$ [ $L_\odot$ ]	$ \dot{M} [10^{-5} M_\odot \text{ yr}^{-1}]$		
			SMC	LMC	solar
0.8	2400	10000	2.19 <sup>(2)</sup>	1.03	5.45
0.8	2600	8000	2.75	3.31 <sup>(1)</sup>	2.38
0.8	2600	10000	5.14	8.18 <sup>(1)</sup>	3.57
0.8	2800	10000	2.88	4.58	2.33 <sup>(1)</sup>
0.8	2800	12000	4.69	6.74	3.23
0.9	2800	10000	1.92	3.17 <sup>(1)</sup>	1.94
1.0	2600	10000	1.19	3.81 <sup>(1)</sup>	2.19 <sup>(1)</sup>

### 3.2. Comparison of models with different element abundances

Generally, when comparing the Magellanic Cloud (MC) models to the solar ones with identical input parameters one finds lower final outflow velocities and lower dust-to-gas ratios. The radiative (in terms of the gravitational) acceleration is weaker as well. For the mass-loss rate, there are input parameters where the MC models show higher values than the corresponding solar ones, as can be seen in table 3. The fact that one finds higher outflow velocities with increasing heavy element abundance, and mass-loss rates of the same order of magnitude is not surprising considering results from basic stellar wind theory. The same behaviour is seen assuming an isothermal wind with an outward directed  $r^{-2}$  force applied outside the critical point. There the mass-loss rate is set as long as the force is only acting in the supersonic regime, that is outside the critical point.

Typically the outflow velocities of the solar metallicity models are higher by about a factor of 2.2( $\pm 0.2$ ) than those of the LMC, and 4( $\pm 1$ ) than those of the SMC. The dust-to-gas ratios are higher by about a factor of 1.3( $\pm 0.1$ ) and 2.3( $\pm 0.2$ ), re-

spectively. For the acceleration the trend is less clear, i.e. the data show a wider spread, especially in the SMC case. The solar abundance models produce values higher by a factor of 3.6( $\pm 1.2$ ), and 5.8( $\pm 1.2$ ), respectively.

Figure 1 depicts the radial structure of the model with  $M = 0.9 M_\odot, T_\star = 2800 \text{ K}, L = 10^4 L_\odot, P = 600 \text{ d}, \Delta v = 5 \text{ km s}^{-1},$  and  $\epsilon_{C/O} = 1.8$  for SMC, LMC, and solar abundances at the instant of 90 periods after starting the model calculation. It gives a good representation of these trends, especially for the outflow velocity and the dust density, recalling that they are not only time but as well radial averages. The acceleration trend is more indirectly represented, since the graph is a time snapshot, but the acceleration average is a time average of the value at the radius of the first maximum of the condensation degree.

In the lowest panels two more trends can be seen. The condensation degree which is closely related to the dust-to-gas ratio by mass according to  $\rho_d/\rho_g \propto \epsilon_O(\frac{\epsilon_C}{\epsilon_O} - 1)f_c$  (see eq. (4.7) of Winters, 1994) is less pronounced and more irregular in LMC and SMC models than in solar models. While in this solar metallicity model the condensation degree is virtually 1 in the dust shells, the SMC model only reaches maximum value of about 0.8. That is all the condensable material is accumulated in dust grains in the solar model, but with lower metallicity the condensation is less efficient. The second trend resulting from this simple graphical comparison of respective models concerns the average grain size. In the SMC case the grains reach much larger radii than with solar abundances. Since the nucleation rate drops with decreasing metal abundance, there are fewer grains in that case to collect the available C atoms. Additionally, the grains have more time for growing due to their lower velocity, hence they become larger.

### 3.3. Approximative mass-loss formulae

To give a mass-loss description applicable to stellar evolution we restrict our model set to those of type A, describing stable dust-driven wind. These are characterised by the criterion  $\langle\alpha\rangle_t > 1.$

Furthermore, one has to consider the treatment of the “mechanical” input parameters  $\Delta v$  and  $P$  as well as the C/O abundance ratio for this purpose. Fortunately, the models are most sensitive to the stellar parameters luminosity  $L,$  effective temperature  $T,$  and mass  $M$  (for the solar metallicity models already pointed out by Arndt et al., 1997). Therefore, we followed for the LMC and SMC models the same approach as for solar metallicity models (Wachter et al., 2002) and fixed the velocity amplitude  $\Delta v$  to a value of  $5 \text{ km s}^{-1}.$  Setting the abundance ratio  $\epsilon_{C/O}$  to 1.8 allows for the fact that it has to be high enough to produce a stable wind without being unreasonable.

Concerning the period  $P$  we relied on observed period-luminosity relations of LPVs. Wachter et al. (2002) took the dependence of the mass-loss rate on the period into account by transferring the slight  $P$  dependence to an additional luminosity term. Now, we take the period dependence more directly into account by choosing only those models where the  $P$ - $L$  relation (Groenewegen & Whitelock, 1996) is fulfilled. This is possible since we now have a larger set of models at hand.

For the selected LMC models a multi-linear least square fit of the form  $\log \dot{M} = a_0 + a_1 * \log x_1 + \dots$  was performed leading to the following formula:

$$|\dot{M}[M_\odot \text{ yr}^{-1}]| = 3.80 \times 10^{-5} \times (M_\star[M_\odot])^{-2.56} \times \left(\frac{T_\star[\text{K}]}{2600}\right)^{-7.44} \times \left(\frac{L_\star[L_\odot]}{10^4}\right)^{2.86} \quad (1)$$

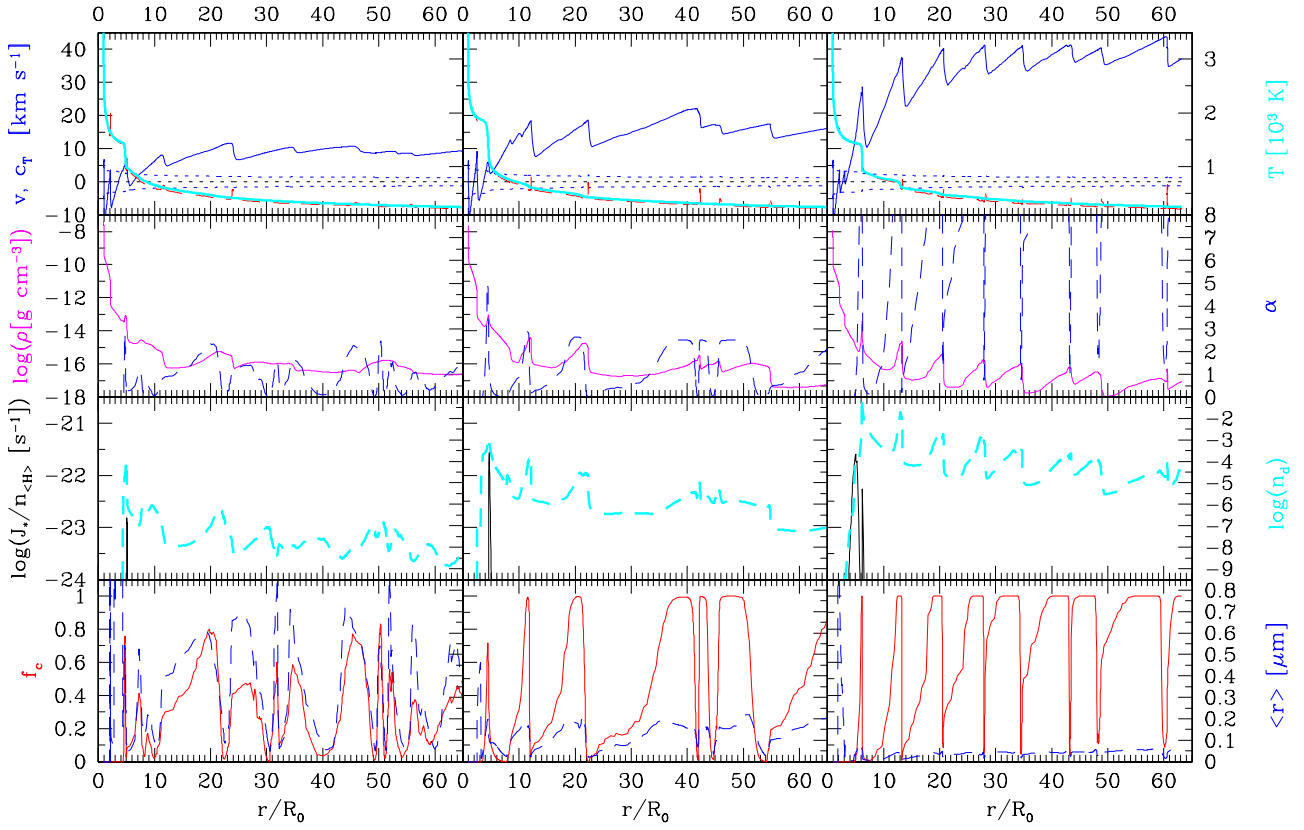


**Fig. 1.** SMC (left), LMC (middle), and solar (right) model with identical input parameters  $M = 0.9 M_{\odot}$ ,  $T_{\star} = 2800$  K,  $L = 10^4 L_{\odot}$ ,  $P = 600$  d,  $\Delta v = 5$  km s $^{-1}$ ,  $\epsilon_{\text{C}}/\epsilon_{\text{O}} = 1.8$ . Shown is the radial structure at time  $t = 90 P$ ,  $R_0$  being the stellar radius at the start of the calculation  $t = 0 P$ . The depicted quantities are (left scales) the radial velocity  $v$  (solid blue line), the speed of sound  $c_T$  (dotted blue lines – in-/outwards, zero line as guide to the eye), the density  $\rho$  (solid magenta), the nucleation rate per hydrogen atom  $J_{\star}/n_{\text{H}}$  (solid black), and the degree of condensation  $f_c$  of the dust (solid red), (right scales) the gas temperature (dashed red) and equilibrium temperature  $T$ , the ratio of radiative to gravitational acceleration  $\alpha$  of the material (dashed blue), the dust density  $n_d$  (dashed cyan), and the mean dust particle radius  $\langle r \rangle$  (dashed blue).

with a correlation coefficient of  $K = 0.98$ .

For the SMC models the result is:

$$|\dot{M}[M_{\odot} \text{ yr}^{-1}]| = 2.34 \times 10^{-5} \times (M_{\star}[M_{\odot}])^{-3.01} \times \left(\frac{T_{\star}[\text{K}]}{2600}\right)^{-6.22} \times \left(\frac{L_{\star}[L_{\odot}]}{10^4}\right)^{2.84} \quad (2)$$

with a correlation coefficient of  $K = 0.97$ .

The formula for solar element composition as published in Wachter et al. (2002) reads, for comparison:

$$|\dot{M}[M_{\odot} \text{ yr}^{-1}]| = 4.52 \times 10^{-5} \times (M_{\star}[M_{\odot}])^{-1.95} \times \left(\frac{T_{\star}[\text{K}]}{2600}\right)^{-6.81} \times \left(\frac{L_{\star}[L_{\odot}]}{10^4}\right)^{2.47} \quad (3)$$

where the correlation coefficient is  $K = 0.97$ .

As already pointed out for the solar metallicity case, the most influential parameter in the formulae for LMC/SMC abundances is again the effective temperature. This reflects the extreme sensitivity of the dust nucleation with respect to the local temperature.

Graphical illustrations of the formulae for LMC and SMC are given in figure 2 for a fixed mass of  $M_{\star} = 1.0 M_{\odot}$ , temperature range of 2400 ... 3000 K, and luminosity of 5000 ... 15000  $L_{\odot}$ . The lines on the base of the diagrams are projections of contour lines, i.e. they mark those temperature and luminosity

values for which the resulting mass-loss rate is  $10^{-4}$ ,  $5 \times 10^{-5}$ ,  $10^{-5}$ , and  $5 \times 10^{-6} M_{\odot} \text{ yr}^{-1}$ , respectively. These show that for the SMC higher luminosities / lower temperatures are necessary to reach the same mass-loss rate as in the LMC.

To give the validity limit of the above formulae the selection criterion needs to be expressed in terms of the stellar parameters, since  $\langle \alpha \rangle$  is a quantity which does not appear in stellar evolution calculations. By considering the ratio  $L/M$  over temperature  $T$  for each metallicity set it turns out that the criterion can be approximated using  $\frac{L}{M} \propto T^x$ . We find that equations (1) and (2) are valid for

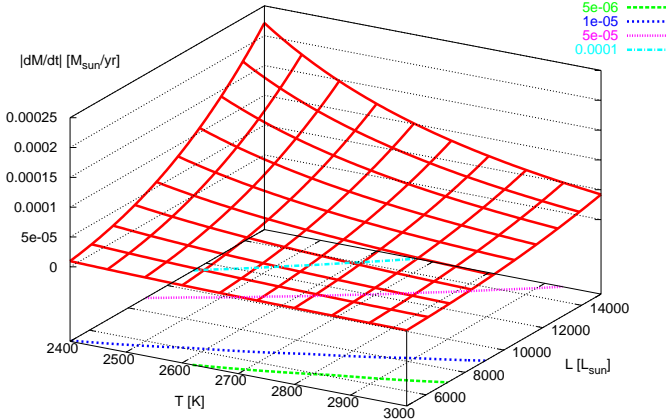
$$L > L_{\text{crit}} \quad , \quad L_{\text{crit}} = \begin{cases} 5.58 \times 10^{-8} T^{3.198} M, & \text{LMC} \\ 5.47 \times 10^{-4} T^{2.126} M, & \text{SMC} \end{cases} \quad (4)$$

The need to include such precise values of the temperature exponent expresses again the steep dependence of the dust nucleation rate on the local kinetic gas temperature.

#### 4. Results from application to stellar evolution

In order to get some insight into the overall mass loss of subsolar metallicity stars on the AGB compared their solar counterparts, we applied the derived mass-loss rates to stellar evolution calculations. For that purpose, we used again the well-calibrated

(a) LMC:



(b) SMC:

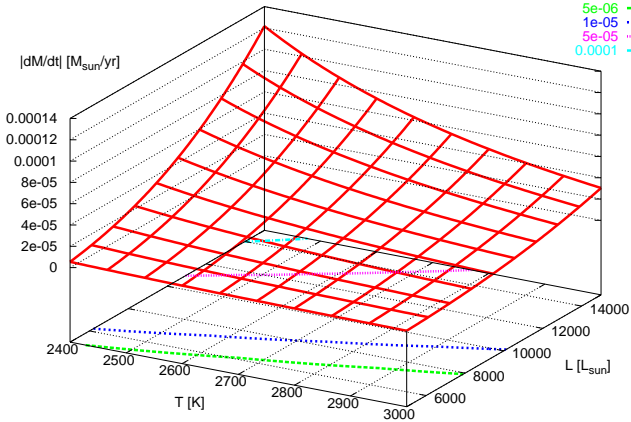


**Fig. 2.** Graphical illustration of the fit formulae for the mass loss rate for fixed mass  $M_{\star} = 1.0 M_{\odot}$ .

Cambridge evolution code (cf. Wachter et al., 2002, and references therein), as we did for the solar metallicity models. A particular advantage of these evolution models is a good match of their effective temperatures for stars high on the AGB, according to a semi-empirical adjustment made by Schröder et al. (1999). This is an important point: Only a small mismatch in  $T_{\text{eff}}$  can result in a significantly different mass-loss rate, despite the use of the very same mass-loss formula, because of the high dependence of the mass-loss on  $T_{\text{eff}}$  of the stellar models.

Mass loss is included by reducing the stellar mass at the outer boundary, whereby the particular formulation depends on the current evolutionary stage of the model. Mass loss is considered only after the star runs out of hydrogen in the core and reaches the red giant branch (RGB). The formulae derived in section 3.3 are valid above the respective critical luminosities. These are reached when the star has developed up to the tip of the AGB and has entered the thermally pulsing phase. Before this phase we apply a formula given by Schröder & Cuntz (2005) who have reconsidered the well-known Reimers formula (Reimers, 1975) by using theoretically motivated arguments. As a result it now includes two new terms containing a dependence on the effective temperature and the surface gravity, respectively. Around  $L_{\text{crit}}$  a short transition zone is introduced where the code interpolates between the modified Reimers and the formula based on dust-driven wind models to avoid artificial jumps in the mass-loss rate.

We have generated model grids with a metallicity of  $Z = 0.01$  and  $Z = 0.001$  to represent LMC and SMC stars, respec-

tively, the closest values for which appropriate necessary input data is available.

Table 4 lists the initial masses and the total mass lost over the whole life of the star, according to a number of our evolution models with mass loss for subsolar metallicity. Within each grid we calculated evolutionary tracks without and with overshooting (with a value of  $\delta_{\text{ov}} = 0.12$  for the overshoot parameter as tested by Schröder et al., 1997).

#### 4.1. Mass loss histories

The temporal development of the stellar mass loss rate is of particular interest, since the density structure of a planetary nebula is determined by the mass-loss history of its progenitor star. Figure 3 shows four examples of such mass-loss histories. Depicted are the rates of  $Z = 0.01$  models with an initial mass of (a)  $M_i = 1.25 M_{\odot}$  and (c)  $M_i = 2.50 M_{\odot}$ , and  $Z = 0.001 M_{\odot}$  models with (b)  $M_i = 1.95 M_{\odot}$  and (d)  $M_i = 2.50 M_{\odot}$ . Each graph is plotted over the final 200 000 years of the stellar life, but the scales of the mass-loss rates differ! The graphs (a) and (b) show the results for the lowest initial mass where the critical luminosity is reached and a brief onset of a dust-driven wind results, respectively, while graphs (c) and (d) show the highest initial mass where the evolution is followed until the star leaves the AGB.

What catches the eye at first glance is the fact that the number of thermal pulses (seen as spikes) increases and the interpulse duration decreases with decreasing metallicity (cf. figures 3(c) and (d)). This finding is in accordance with the predictions of other stellar evolution calculations using different mass loss prescriptions, see for example Marigo (2001), and references therein. As pointed out there, the exact number of thermal pulses depends on the chosen mass-loss formalism.

Another clear difference is the overall shape of the mass-loss histories of models with different metallicity: The  $Z = 0.01$  graph resembles the mass-loss rates of our models with solar metallicity, see figures 2–5 in Wachter et al. (2002). For these metallicities the critical luminosities are fairly similar and the stars reside in a regime above that value while they are in the thermally pulsing AGB phase. As a result the mass loss in this late evolutionary stage is controlled by our formula based on dust-driven winds. By contrast, the  $Z = 0.001$ ,  $M = 2.5 M_{\odot}$  rate is mostly dominated by not dust-driven mass-loss, here described by the modified Reimers law. Only during the last few thermal pulses does the star reach luminosities high enough for the dust-driven wind formula to apply. Our present models for SMC-like metallicity therefore result in a rather smooth and broad density distribution of the blown-out material developing to a planetary nebula<sup>1</sup>. Models with solar and LMC abundances though have distinctly higher mass-loss rates during the last  $\sim 25$  000 years leading to a denser and narrower mass distribution.

#### 4.2. Total masses lost

The total mass lost by a star in the course of its evolution, for given initial stellar mass, is an important quantity in modelling the galactic chemical evolution. A further quantity of interest is the mass of the resulting white dwarf (WD) or, rather, the WD mass distribution, since WDs are considered to be the end-products of stellar evolution for intermediate masses. The final

<sup>1</sup> Naturally, this is a simplified picture, since it disregards different velocities with which the material might be driven away.

**Table 4.** Stellar evolution grids: final masses and ages

$M_i$ [ $M_\odot$ ]	Z=0.01				Z=0.001			
	$\delta_{ov} = 0$		$\delta_{ov} = 0.12$		$\delta_{ov} = 0$		$\delta_{ov} = 0.12$	
	$M_e$ [ $M_\odot$ ]	age [ $10^9$ yr]	$M_e$ [ $M_\odot$ ]	age [ $10^9$ yr]	$M_e$ [ $M_\odot$ ]	age [ $10^9$ yr]	$M_e$ [ $M_\odot$ ]	age [ $10^9$ yr]
0.70					0.47	24.24	0.47	24.33
0.75					0.49	18.83	0.49	18.91
0.80	0.47	23.77	0.47	23.79	0.50	14.88	0.50	14.95
0.85	0.48	19.02	0.48	19.04	0.53	12.06	0.54	12.14
0.90	0.49	15.41	0.49	15.43	0.55	9.85	0.56	9.92
0.95	0.53	12.73	0.53	12.73	0.57	8.15	0.57	8.21
1.00	0.55	10.53	0.55	10.54	0.58	6.82	0.59	6.88
1.05	0.56	8.80	0.56	8.83	0.59	5.78	0.60	5.83
1.10	0.57	7.42	0.57	7.48	0.59	4.94	0.60	4.99
1.15	0.58	6.31	0.58	6.40	0.60	4.26	0.61	4.32
1.20	0.59	5.42	0.58	5.53	0.61	3.70	0.62	3.77
1.25	0.59	4.70	0.59	4.80	0.62	3.24	0.63	3.31
1.30	0.60	4.11	0.59	4.19	0.63	2.86	0.64	2.93
1.35	0.60	3.61	0.60	3.69	0.63	2.54	0.64	2.61
1.40	0.61	3.19	0.60	3.26	0.64	2.26	0.65	2.34
1.45	0.61	2.85	0.61	2.92	0.65	2.03	0.66	2.11
1.50	0.62	2.55	0.61	2.62	0.66	1.83	0.67	1.92
1.55	0.62	2.29	0.61	2.37	0.66	1.65	0.67	1.75
1.60	0.63	2.07	0.62	2.16	0.67	1.50	0.68	1.61
1.65	0.63	1.87	0.63	1.98			0.69	1.49
1.70	0.64	1.70	0.63	1.82			0.69	1.38
1.75	0.64	1.55	0.64	1.67			0.70	1.35
1.80	0.65	1.43	0.64	1.55			0.70	1.27
1.85	0.65	1.32	0.65	1.44			0.71	1.19
1.90	0.66	1.22	0.66	1.37			0.72	1.10
1.95	0.66	1.14	0.66	1.46			0.73	1.03
2.00	0.67	1.06	0.67	1.36			0.74	0.96
2.05	0.67	1.00	0.67	1.27			0.75	0.90
2.15	0.68	0.90	0.68	1.12			0.77	0.79
2.25	0.69	0.82	0.69	0.99			0.79	0.70
2.35			0.71	0.88			0.81	0.62
2.50							0.85	0.53

stellar (WD) mass is basically identical with the core mass of the AGB star supposing that the whole envelope is ejected via stellar winds. Therefore we present in the following the total (integrated over the whole stellar life) masses lost by stars with subsolar metallicity, according to our models.

Figure 4 depicts the amount of mass lost by a star of given initial mass  $M_i$  during its life for the two grids of tracks with metallicity (a)  $Z = 0.01$  and (b)  $Z = 0.001$ . In addition, we detail the time-integrated mass-loss of the RGB and AGB phases. In both graphs the respective masses lost by models with solar metallicity (and same initial mass) are plotted as well, for comparison. It can be seen in figure 4(a) that the total amount of mass loss is virtually the same, but not lower for LMC-like than for solar abundances. However, the contributions lost on the RGB and AGB are shifted, especially for the lower initial masses shown more mass is already lost in the RGB phase. For  $Z = 0.001$  figure 4(b) shows that the total amount of mass lost is almost the same as for solar metallicity for the lower end of initial masses. With higher initial mass though, less material is blown away for SMC-like abundances. Again there is a shift towards higher contribution of the RGB, but less pronounced than in case (a).

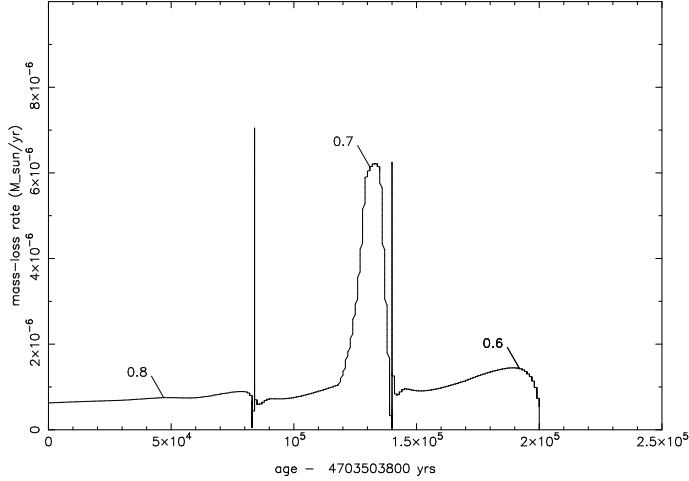
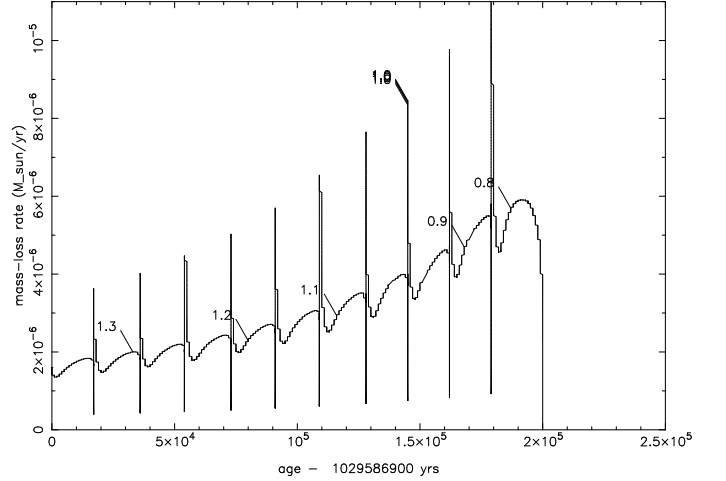
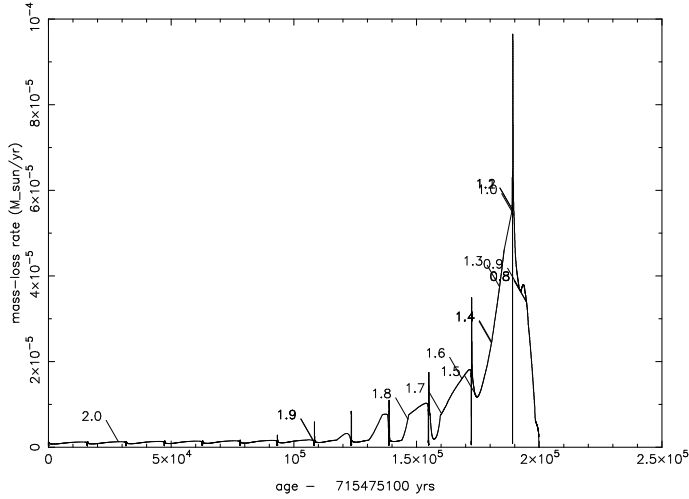
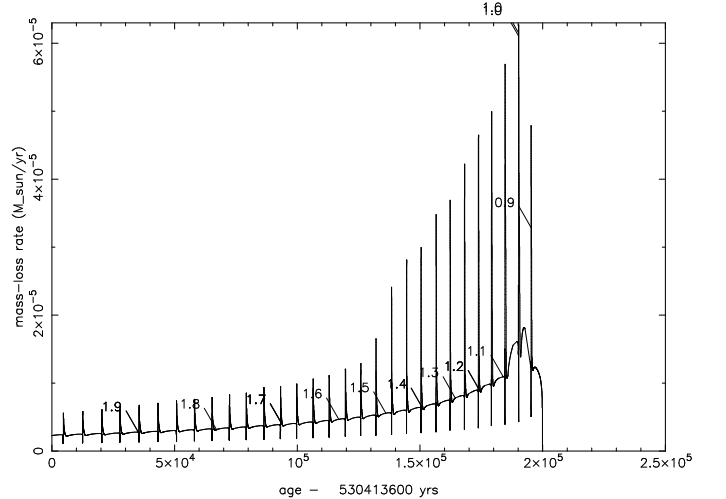
## 5. Discussion

In order to account for carbon-rich chemistry, we enhance the carbon element abundance considering the C/O ratio as a model parameter. In this work we considered mainly values of 1.3

and 1.8, the latter especially in models with SMC abundances. This value might be regarded as rather extreme. Nevertheless, Matsuura et al. (2005) reported possible C/O values of  $\sim 1.4$  for LMC stars and even higher for the SMC, resulting from a chemical equilibrium model to explain the strength of observed  $C_2H_2$  absorption features.

Van Loon et al. (2005) observed AGB stars in the Large Magellanic Cloud, C-stars as well as M-type stars, and derived mass-loss rates of  $\log \dot{M}[M_\odot \text{ yr}^{-1}] \sim -5.6 \dots -5$  for C-type and  $\sim -5 \dots -4.2$  for M-type giants. Furthermore, they give an empirical mass-loss formula for these stars dependent on effective temperature and luminosity and compare their formula to equation (3) derived from our models with solar abundances. Even though the dependence of our LMC formula on effective temperature is stronger, it is consistent with their observed value within the errors. Furthermore, they argued that even if their observed luminosity dependence is much lower than our theoretical value, they may still be consistent as the effect of decreasing mass-loss rate with increasing stellar mass counteracts the luminosity dependence.

An issue which remains uncovered by the models presented here is related to the assumption of grey radiative transfer and its effect on the resulting mass-loss rates. Höfner et al. (2003) included frequency-dependent treatment in their models and found those to have cooler and denser upper layers which is in favour of a more efficient dust condensation. A radiative pressure 2–3 times larger than the grey values results, and the mass-loss

(a)  $Z = 0.01$ ,  $M_i = 1.25 M_\odot$ :(b)  $Z = 0.001$ ,  $M_i = 1.95 M_\odot$ :(c)  $Z = 0.01$ ,  $M_i = 2.50 M_\odot$ :(d)  $Z = 0.001$ ,  $M_i = 2.50 M_\odot$ :**Fig. 3.** Mass loss histories of stars with different initial masses and metallicities. Labels denote the current mass.

rates and wind velocities are larger in the non-grey case for the three models compared to grey ones calculated with Planck-mean opacities. On the other hand, Helling et al. (2000) investigated the effects of molecular opacities on the characteristics of carbon-rich dust driven wind models in the frame work of grey opacities. These authors compared opacities represented by the same constant value used here, with Rosseland-mean and Planck-mean averages. As a general result it is found that the mass loss rates and wind velocities are highest for the constant value of the opacity also used here and lowest for the Planck-mean opacities, whereas the Rosseland-mean leads to intermediate values of the mass loss rate. Considering these results and the results of Höfner et al. (2003) it is to be expected that the inclusion of non-grey opacities in our models may lead to somewhat reduced mass-loss rates and wind velocities. A quantitative assessment of the effect would however require the calculation of an appropriate set of models with non-grey treatment of the gas opacities for the sub-solar element abundances discussed here.

Concerning the comparison of hydrodynamical wind models with different element compositions Mattsson et al. (2008) suggest that one should rather keep the abundance difference C/O fixed than the ratio C/O, since for dust formation the amount of free carbon is important assuming complete CO blocking. Doing so effectively leads to higher C/O ratios for lower metallicity

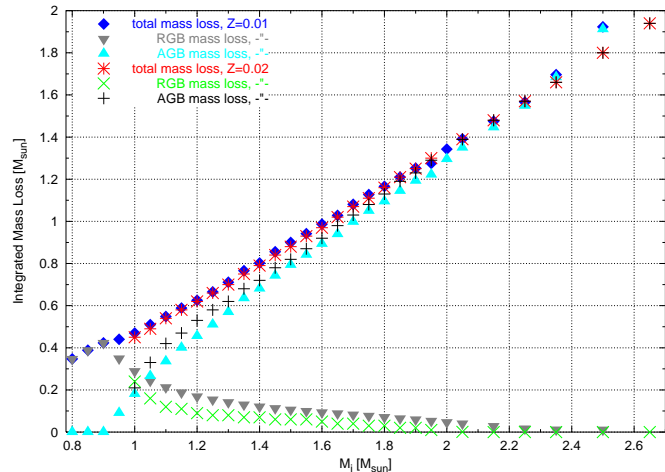
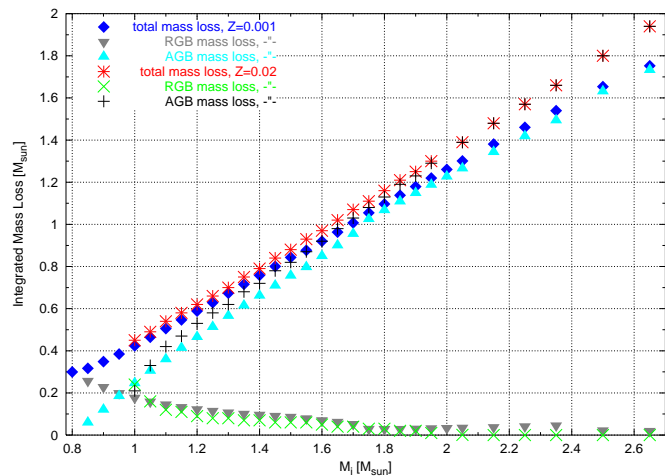
where the oxygen abundance is decreased as well. For the mass-loss rates this different approach of comparing models consequently has not much influence, since the models with higher C/O are even further beyond the threshold. For example, we calculated the LMC and SMC model shown in figure 1 with fixed C-O ( $\log_{10}(\epsilon_C - \epsilon_O) \sim 8.72$ )<sup>2</sup> instead C/O. This leads to averaged mass-loss rates reduced by a factor of 0.7 and raised by a factor 1.3 (to the value with fixed C/O), respectively. Considering the hydrodynamical structure itself, the models with fixed C-O are very similar to their solar counterparts, e.g. they show velocities of the same order and the degree of condensation reaches 100% in the dust shells even in the SMC model.

Despite the differences in the assumptions of gas opacities and radiative transfer we come to the same conclusion about mass loss as Mattsson et al. (2008): Lower metallicities do not necessarily result in lower mass-loss rates.

As stated before the wind models predict higher critical luminosities for a dust-driven wind to develop for SMC abundances than for the LMC, e.g. a factor of 1.7 at  $\log T = 3.5$ . On the other hand, stellar evolution tracks of stars with  $Z = 0.001$  reach higher luminosities (up to 0.2 dex) at the tip of the AGB

<sup>2</sup> which corresponds to values of C/O  $\sim 3.4$  and  $5.9$ , respectively



(a) Models with metallicity  $Z = 0.01$ :(b) ...and  $Z = 0.001$ :

**Fig. 4.** Integrated mass loss as a function of initial mass. For each initial mass the total mass loss is shown (blue diamonds) as well as the respective fractions lost on the RGB (cyan) and the AGB (grey). For reference the respective solar values are given as well in both plots (red, green, and black crosses).

than their  $Z = 0.01$  counterparts with same initial mass. In other words our models predict SMC stars to undergo mass loss due to dust-driven winds, at least those with initial masses of about two solar masses and higher, despite the higher critical luminosity required to do so.

## 6. Conclusions

In this article we present dust-driven wind models with subsolar metallicities as observed in the Magellanic Clouds. These are calculated using an adapted version of the hydrodynamical code developed at the Technical University Berlin, with a radiative transport description improved for lower opacities. Based on a grid of models for SMC and LMC metallicity respectively, we derived approximative mass-loss formulae valid above a critical luminosity, that is on the tip of the AGB. In order to investigate the overall stellar mass loss we applied these descriptions to stellar evolution using the Cambridge code.

Our main results can be summarised as follows:

1. A comparison of the subsolar metallicity models to the corresponding solar ones with fixed C/O ratio reveals that typically the outflow velocities of the solar models are higher by about a factor of 2.2 than those of the LMC, and a factor of 4 higher than those of the SMC. This is because in the solar metallicity case a larger amount of dust is formed which can more efficiently accelerate the wind outside of the sonic region.
2. The averaged mass-loss rates of these models are of the same order of magnitude as the solar ones. This can be understood by the threshold character of the radiative acceleration in a dust-driven wind: Only a moderate amount of dust is needed to form in the sub-sonic wind region to accelerate the wind to super-sonic velocities (equivalent to  $\alpha > 1$  at sub-sonic velocities). The mass-loss rate is in this case determined in the sub-sonic region, irrespective of how much additional dust is still formed further out in the wind.
3. The most influential parameter in the mass-loss formulae is the temperature hinting at the sensitive dependence of the dust formation to this quantity.
4. Once the abundance ratio C/O is above a lower limit it still has an impact on the hydrodynamical structure of the models, e.g. different outflow velocities, but the averaged mass-loss rate does not change dramatically anymore. Again this is plausible due to characteristics of the driving force in a radiation driven wind (see also section 3.2).
5. While LMC and solar abundance wind models result in fairly equal critical luminosities necessary to drive a wind by radiation pressure on dust, higher values are required in the SMC models. Since stellar evolution models with lower metallicity reach higher luminosities on the tip of the AGB, some of these stars (with initial masses  $M_i \gtrsim 2M_{\odot}$ ) suffer dust-driven mass loss nevertheless.

*Acknowledgements.* We thank S. Höfner and L. Mattsson for discussions about their hydrodynamical models in general, and for insights into effects of non-grey radiative transfer in particular. Part of this work was supported by the German *Deutsche Forschungsgemeinschaft, DFG* project number Se 420/22. KPS would like to acknowledge support by Conacyt (grant No. 57744).

## References

- Arndt, T. U., Fleischer, A. J., Sedlmayr, E., 1997, *A&A* 327, 614  
 Cioni, M.-R. L., Marquette, J.-B., Loup, C., Azzopardi, M., Habing, H. J., Lasserre, T., Lesquoy, E., 2001, *A&A*, 377, 945  
 Eggleton, P. P., 1973, *MNRAS* 163, 279  
 Fleischer, A. J., Gauger, A., Sedlmayr, E., 1992, *A&A* 266, 321  
 Fleischer, A. J., 1994, PhD thesis, Technische Universität, Berlin, Germany  
 Gail, H.-P., Sedlmayr, E., 1988, *A&A* 206, 153  
 Gauger, A., Gail, H.-P., Sedlmayr, E., 1990, *A&A* 235, 345  
 Groenewegen, M. A. T., Whitelock, P. A., 1996, *MNRAS* 281, 1347  
 Helling, Ch., Arndt, T. U., Sedlmayr, E. 2002, in: *ASP Conf. Ser. 259: IAU Colloq. 185: Radial and Nonradial Pulsations as Probes of Stellar Physics*, (eds.) Aerts, C., Bedding, T. R., Christensen-Dalsgaard, J., 546  
 Helling, C., Winters, J. M., Sedlmayr, E., 2000, *A&A* 358, 651  
 Höfner, S., Gautschy-Loidl, R., Aringer, B., Jørgensen, U. G., 2003, *A&A* 399, 589  
 Jeong, K. S., Winters, J. M., Le Bertre, T., Sedlmayr, E., 2003, *A&A* 407, 191  
 Marigo, P., 2001, *A&A* 370, 194  
 Matsuura, M., Zijlstra, A. A., van Loon, J. T., Yamamura, I., Markwick, et al., 2005, *A&A* 434, 691  
 Mattsson, L., Wahlin, R., Höfner, S., Eriksson, K., 2008, accepted by *A&A*  
 Reimers, D., 1975, *MSRSL* 8, 369  
 Schirmacher, V., Witke, P., Sedlmayr, E., 2003, *A&A* 404, 267  
 Schröder, K.-P., Cuntz, M., 2005, *ApJ* 630, L73  
 Schröder, K.-P., Pols, O. R., Eggleton, P. P. 1997, *MNRAS* 285, 696  
 Schröder, K.-P., Winters, J.-M., Sedlmayr, E., 1999, *A&A* 349, 898  
 van Loon, J. T., Cioni, M.-R. L., Zijlstra, A. A., Loup, C., 2005, *A&A* 438, 273  
 Wachter, A., Schröder, K.-P., Winters, J. M., Arndt, T. U., Sedlmayr, E., 2002, *A&A*, 384, 452



- Winters, J. M., 1994, PhD thesis, Technische Universität, Berlin, Germany  
Winters, J. M., Fleischer, A. J., Gauger, A., Sedlmayr, E., 1994, A&A 290, 623  
Winters, J. M., Le Bertre, T., Jeong, K. S., Helling, Ch., Sedlmayr, E., 2000,  
A&A 361, 641